ACS APPLIED MATERIALS & INTERFACES

Research Article

www.acsami.org

Solution Processed ZnO Hybrid Nanocomposite with Tailored Work Function for Improved Electron Transport Layer in Organic Photovoltaic Devices

Yun-Ju Lee,* Jian Wang, Samuel R. Cheng, and Julia W. P. Hsu

Department of Materials Science and Engineering, University of Texas at Dallas, 800 West Campbell Road, Richardson, Texas 75080, United States

ABSTRACT: We demonstrate improved organic photovoltaic device performance using solution processed electron transport layers of ZnO nanoparticle (NP) films containing organic additives, poly(vinylpyrrolidone) (PVP), or diethanolamine (DEA), that do not require post processing after film deposition. Inclusion of PVP or DEA decreased the ZnO work function by 0.4 eV through interfacial dipole formation. While PVP did not change the ZnO NP shape or size, DEA modified the ZnO shape from 5 nm × 15 nm nanorods to 5 nm nanoparticles. At an optimized PVP concentration of 0.7 wt %, ZnO NP:PVP electron transport layers (ETLs) improved the efficiency of inverted P3HT:PCBM devices by 37%, primarily through higher fill factor. ZnO NP:PVP and ZnO NP:DEA ETLs increased the open circuit voltage of inverted P3HT:ICBA devices by 0.07 V due to decreasing ETL work function, leading to enhanced built-in field. The relationship between ZnO nanocomposite ETL work function, donor−acceptor energy offset, and device performance is discussed. The effects of the two additives are compared.

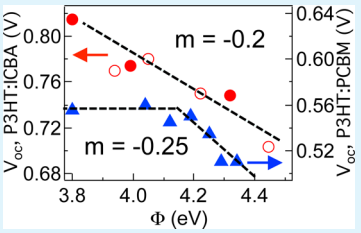

KEYWORDS: *organic photovoltaics, transport layer, ZnO nanoparticles, hybrid nanocomposites*

INTRODUCTION

Interfacial contact layers between the active layer and electrodes of organic photovoltaic (OPV) devices have demonstrated improved performance, as summarized by two recent reviews.[1,2] Solution processed interfacial contact layers for OPV devices have generated a significant research effort due to their promise to eliminate costly vacuum deposition steps and their compatibility with inexpensive fabrication procedures such as roll-to-roll processing.[2] However, significant processing challenges arise from, e.g., solvent orthogonality, wetting of underlying layers, and low-temperature processing (<100 °C). Oxide films are commonly made from sol-gel precursors that require processing temperatures higher than 300 °C, which precludes processing on top of OPV active layers. Currently, only a few low-temperature solution processed electron transport layers (ETLs) have been reported, such as TiO_x sol-gel films[3−5] and ZnO nanoparticles (NPs),[6−8] which increased the power conversion efficiency (η) of OPV devices. ETLs consisting of dielectric polymer films[9−11] also improved OPV performance through a decrease in work function (Φ) due to interfacial dipoles, although film thicknesses are limited to <10 nm to avoid high series resistance (R_s). To take advantage of both Φ reduction and low R_s, several groups have fabricated bilayers[12] and blends[13,14] of semiconducting inorganic oxides and dielectric polymers as ETLs. Jo et al. synthesized ZnO NP suspensions, added different concentrations of poly(ethylene oxide) (PEO), and spin coated mixture on top of a poly(3-hexylthiophene):[6,6]-phenyl-C61-butyric acid methyl ester (P3HT:PCBM) bulk heterojunction (BHJ) active layer as ETL in a conventional architecture.[13] They observed a significant increase in device fill factor (FF) and smaller increases in short circuit current density (J_{sc}) and open circuit voltage (V_{oc}) as PEO concentration increased up to 5 wt %, and attributed the enhancement to lowering of ZnO electron affinity with PEO that leads to Ohmic contact with Al. Small et al. annealed a spin coated film of mixed poly(vinylpyrrolidone) (PVP) with ZnO sol-gel precursor at 200 °C to make ETL for inverted OPV devices, and observed a significant increase in FF but only after UV-ozone treatment of the ZnO:PVP blend film to remove excess PVP.[14] Self-assembled monolayers deposited on ZnO NP films have been shown to affect the performance of OPV devices through formation of interfacial dipoles.[6−8]

Here, we report the room temperature solution processing of ZnO NP hybrid nanocomposite films using suspensions of ZnO NP synthesized in the presence of PVP and diethanolamine (DEA) by microwave heating. While PVP had little effect on ZnO NP size or shape, addition of 0.005 M DEA to the reaction solution reduced aggregation and formed spherical NPs. Φ of the nanocomposite can be tuned between 4.4 and 3.95 eV by varying PVP and DEA concentrations. AFM data of ZnO NP:PVP films show that PVP fills in the voids between ZnO NPs at low concentrations, and covers the ZnO NPs at high concentrations. This behavior explains the initial increase and subsequent decrease in FF with increasing PVP concentration for inverted P3HT:PCBM BHJ OPV devices using ZnO NP:PVP films as ETLs. ZnO:PVP films also worked well as ETLs on top of P3HT:PCBM in conventional devices.

Received: June 27, 2013
Accepted: August 27, 2013
Published: August 27, 2013

 © 2013 American Chemical Society dx.doi.org/10.1021/am402511t | *ACS Appl. Mater. Interfaces* 2013, 5, 9128−9133

Finally, inverted P3HT:indene C_{60} bis-adduct (ICBA) devices using ZnO NP:PVP and ZnO NP:DEA films as ETLs exhibited monotonically increasing V_{oc} as Φ decreased, although the weak dependence suggests Fermi level pinning between acceptor and ETL. The synthesis of nanoparticle:organic hybrid nanocomposite films represents a simple and effective method to fabricate interfacial contact layers with tunable Φ and improved OPV device performance.

EXPERIMENTAL SECTION

ZnO NP:PVP and ZnO NP:DEA samples were synthesized by microwave heating using a procedure modified from the literature.[15] For ZnO NP:PVP, solutions of 0.1 M zinc acetylacetonate hydrate (Gelest) and 0−2.8 wt % PVP (MW = 10 kDa, Sigma-Aldrich) in *n*-butanol were heated to 160 °C for 15 min in a single mode 2.54 GHz microwave cavity (CEM Discovery SP) to form NP suspensions. For ZnO NP:DEA, solutions of 0.05 zinc acetylacetonate hydrate and 0−0.01 M DEA (Fisher) were heated to 200 °C for 15 min. Dynamic light scattering (DLS) measurement of NP size was performed using a Malvern Zetasizer Nano ZS. Transmission electron microscopy (TEM) was performed at 200 kV with a JEOL JEM2100. For inverted OPV devices, 20 nm film of ZnO NP:PVP or ZnO NP:DEA film was spin coated on UV-ozone-cleaned (Procleaner Plus, Bioforce Nanoscience) ITO on glass (20 Ω/sq, Thin Film Devices) to act as ETL. The active layer was deposited on the ETL by spin coating at 1200 rpm in N_2 of a solution of P3HT:PCBM (25 mg/mL each) or P3HT:ICBA (25 mg/mL each) in chlorobenzene. After annealing the sample on a hot plate at 170 °C for 10 min in N_2, the MoO_3 hole transport layer (HTL, 5 nm) and Ag (100 nm) were thermally evaporated to complete the device. For conventional OPV devices, the layer sequence consists of ITO, 40 nm of PEDOT:PSS (Heraeus Clevios AI 4083) as the hole transport layer, P3HT:PCBM, ETL of spin coated ZnO NP:PVP, and evaporated Al (100 nm). All devices were 0.11 cm^2 area. Current density−voltage (*J*−*V*) measurement was performed under AM1.5G illumination from a class AAA solar simulator (Abet Technologies) using a low-noise sourcemeter (2635A, Keithley) controlled by a Labview program. Φ was measured in air using a Kelvin probe (Monroe Electronics 244). Topography measurement was performed using an Asylum Research MFP-3D atomic force microscope (AFM).

RESULTS AND DISCUSSION

Morphology and Electronic Properties. Microwave assisted synthesis produced stable suspensions of ZnO NP:PVP and ZnO NP:DEA. TEM images showed that, without organic additive, the ZnP NPs exhibit rod shape with an aspect ratio of ∼3 (Figure 1a and c). PVP has little effect on ZnO NP growth, while DEA strongly influenced ZnO NP size and shape. For example, the ZnO NP sample containing no PVP (Figure 1a) and 0.7 wt % PVP (ZnO NP:PVP (0.7 wt %)) (Figure 1b) both exhibited a rodlike shape, ∼10 nm × 30 nm in size. A high-resolution image of the ZnO NP (Figure 1b, inset) shows a lattice spacing of 0.26 nm along the long axis corresponding to the spacing between (002) planes of ZnO, indicating that it is the *c*-axis. The electron diffraction pattern (Figure 1e) shows three rings, corresponding to nanocrystals with *d*-spacing values of 0.28, 0.26, and 0.25 nm due to diffraction from (100), (002), and (101) planes of wurtzite ZnO. The ZnO NP sample without DEA contained ∼5 nm × 15 nm nanorods (Figure 1c), due to the lower concentration of zinc acetylacetonate hydrate precursor (0.05 M vs 0.1 M) compared to Figure 1a. Addition of 0.005 M DEA instead of PVP to the reaction solution caused the NPs to become spherical in shape, with ∼5 nm size in all directions (Figure 1d). This suggests that strong binding between Zn and DEA

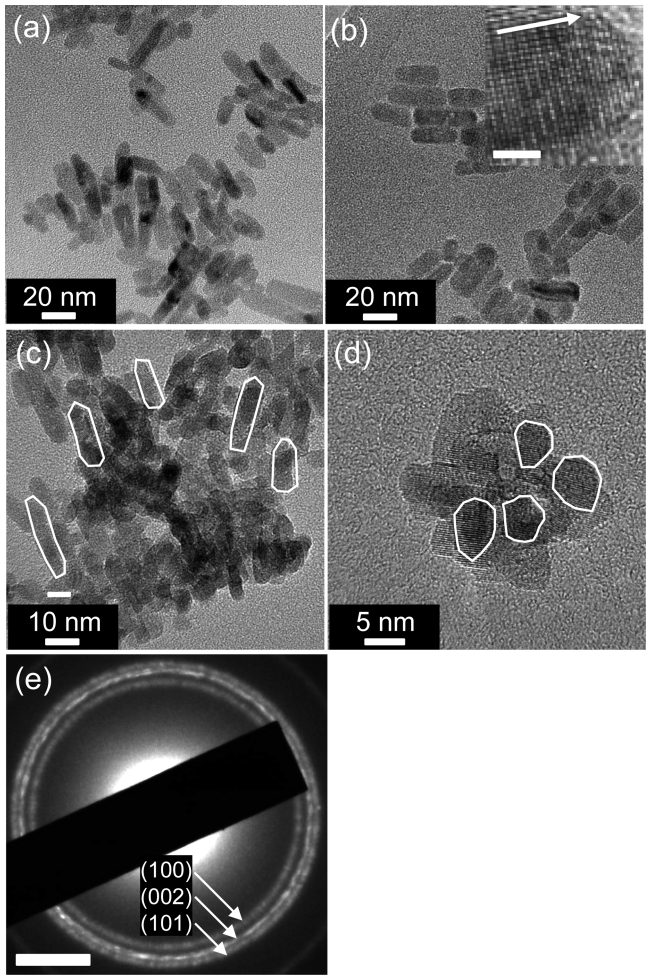

Figure 1. TEM characterization of ZnO NPs synthesized with organic additives. (a) TEM image, no PVP, yielding ∼10 nm × 30 nm nanorods. (b) TEM image, 0.7 wt % PVP, yielding ∼10 × 30 nm nanorods. Inset: high-resolution image of a ZnO NP, showing a lattice spacing of 0.26 nm along the long axis (arrow). (c) TEM image, no DEA, yielding ∼5 nm × 15 nm nanorods. (d) TEM image, 0.005 M DEA, yielding ∼5 nm nanoparticles. Individual nanostructures are outlined in white for clarity. (e) Electron diffraction, 0.7 wt % PVP, with corresponding Miller indices. Scale bar = 2 nm^{-1}.

decreased the growth rate in the *c*-axis direction, leading to isotropic NPs with reduced size. DLS measurements of ZnO NP:PVP suspensions revealed that the hydrodynamic size increased slightly as the PVP concentration increased, from 80 nm without PVP to 130 nm with 1.4 wt % PVP (Figure 2a, red circles). In contrast, the hydrodynamic size of ZnO NP:DEA suspensions decreased as the DEA concentration increased, from 100 nm without DEA to 30 nm with 0.005 M DEA, and remained the same as the DEA concentration was further increased to 0.01 M (Figure 2b, red circles). The decrease in DLS size of ZnO NP:DEA with increasing DEA concentration suggests that DEA acts as a surfactant to limit ZnO NP growth, consistent with TEM results. The TEM images also showed that ZnO NPs formed aggregates, explaining the discrepancy in the sizes obtained from TEM and DLS.

Addition of PVP and DEA to ZnO NPs significantly decreased Φ of the nanocomposite film. While ZnO NP film without PVP has Φ of 4.4 eV, increasing the PVP concentration decreased the Φ values, until a minimum of 3.95 eV was reached for ZnO NP:PVP (0.7 wt %) (Figure 1a, blue

dx.doi.org/10.1021/am402511t | ACS Appl. Mater. Interfaces 2013, 5, 9128−9133

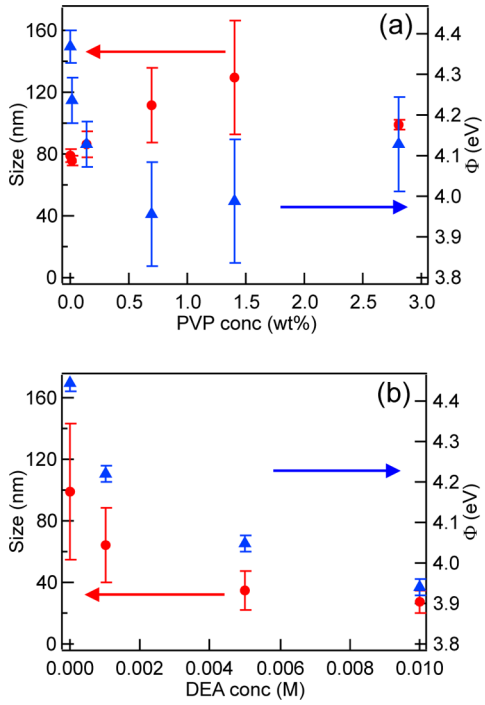

Figure 2. Physical and electronic properties of ZnO NPs synthesized with organic additives. (a) ZnO NP:PVP, showing size from DLS (red circles, left axis) and work function Φ (blue triangles, right axis) as a function of PVP concentration. (b) ZnO NP:DEA, showing size from DLS (red circles, left axis) and Φ (blue triangles, right axis) as a function of DEA concentration. All size and work function measurements were averaged over three separate reactions of ZnO NPs, and the spread represents the standard deviation of the averages of three reactions, instead of the spread in DLS fitting.

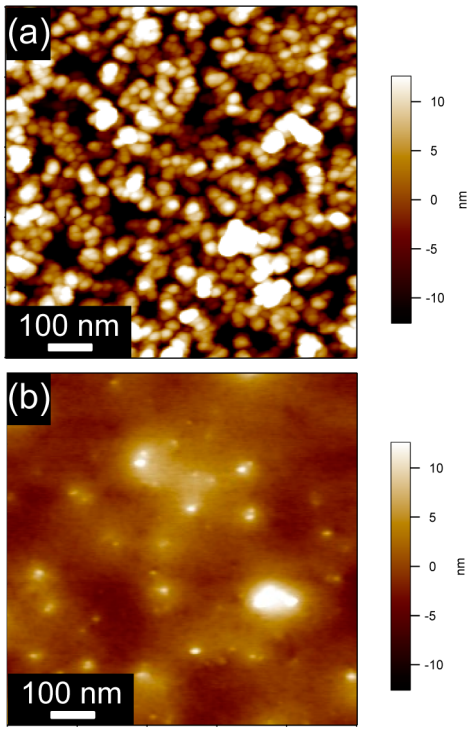

Figure 3. Topography of ZnO NP:PVP films. (a) AFM image of ZnO NP with 0.014 wt % PVP, showing discrete NP features with RMS roughness of 8.9 nm. (b) AFM image of ZnO NP with 2.8 wt % PVP, showing almost complete infiltration with PVP with RMS roughness of 2.7 nm.

triangles). As the PVP concentration increased further to 2.8 wt %, Φ rose to 4.15 eV, matching Φ of pure PVP. The match in Φ suggests that an overlayer of PVP forms above the ZnO NPs, which is caused by filling of voids between ZnO NPs by PVP, as shown below. In comparison, DEA addition monotonically reduced Φ of ZnO NP:DEA to 3.9 eV at 0.01 M DEA (Figure 1b, blue triangles). The reduction in Φ with PVP or DEA addition is most likely caused by interfacial dipole formation between ZnO and the electron donating pyrrolidone or amine group, similar to earlier reports on reduction of Φ for ITO and metals using amine-containing polymers.[10,11] The smaller variation in Φ of ZnO NP:DEA films compared to ZnO NP:PVP films shows that DEA addition produces films with more uniform electronic properties.

An AFM topographic image of ZnO NP containing a small amount of PVP (0.014 wt %) shows discrete 20 and 100 nm features consistent with NPs and aggregates, respectively (Figure 3a). The high root-mean-square (RMS) roughness of 8.9 nm suggests that there is little PVP between the ZnO NPs. By increasing the PVP concentration to 0.7 wt %, the ZnO NP:PVP film exhibits a similar topography (not shown), but the RMS roughness decreased to 7.0 nm, indicating that PVP partially filled in the voids between the ZnO NPs. Finally, the highest PVP concentration (2.8 wt %) ZnO NP:PVP film (Figure 3b) contains few discrete features from NPs or aggregates and a further decrease in RMS roughness to 2.7 nm, suggesting that PVP almost completely covered the ZnO NPs. AFM images of ZnO NP:DEA samples show qualitatively similar results as Figure 3a, due to the smaller concentrations of DEA (0.01 M = 0.13 wt %) compared to PVP, thus not forming an overlayer. In conclusion, PVP fills in the voids between the ZnO NPs and planarizes the nanocomposite film.

OPV Device Performance. Inclusion of ZnO NP:PVP as ETLs resulted in a significant improvement in the performance of inverted OPV devices. *J*−*V* curves of inverted P3HT:PCBM devices at 100 mW/cm^2 intensity (Figure 4a) show that, as the PVP concentration increased from 0 wt % (Figure 4a, black circles) to 0.7 wt % (Figure 4a, green squares), the device V_{oc} increased from 0.51 to 0.56 V and FF increased from 0.47 to 0.60. A plot of device FF (Figure 4b, red circles) and η (Figure 4b, blue triangles) versus PVP concentration shows a high degree of correlation, indicating that the effect of PVP concentration on FF is the primary mechanism for the improvement in device performance. At the same time, the reverse bias saturation current density in the dark decreased significantly as the PVP concentration increased (Figure 4a, inset), so that the shunt resistance (R_p) increased from 31 kΩ cm^2 for the ZnO NP device to 653 kΩ cm^2 for the ZnO NP:PVP (0.7 wt %) device without changes in the series resistance (R_s) (Table 1). The improvement in R_p, FF, and V_{oc} is consistent with filling in of voids between ZnO NPs with PVP, which minimizes shunt formation by eliminating the possibility of direct contact between P3HT:PCBM and ITO through the voids between ZnO NPs. A further increase in PVP concentration to 2.8 wt % (Figure 4a, blue inverted triangles) caused an increase in R_s from 6 to 20 Ω cm^2 and a decrease in FF and J_{sc} (Table 1). This is consistent with the presence of a transport barrier due to the formation of an insulating PVP overlayer above the ZnO NPs, as seen in the AFM image (Figure 3b). Note that the optimal PVP concentration in the ZnO NP:PVP ETL is not because of an optimal work function

dx.doi.org/10.1021/am402511t | ACS Appl. Mater. Interfaces 2013, 5, 9128−9133

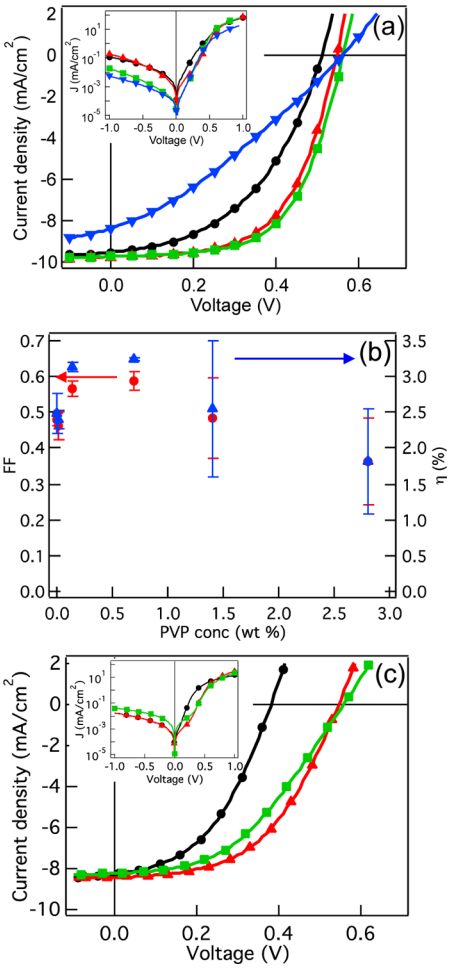

Figure 4. Performance of P3HT:PCBM devices using ZnO NP:PVP as ETL. (a) $J-V$ response at AM1.5G 100 mW/cm^2 for inverted devices using ZnO NP with 0 wt % (black circles), 0.14 wt % (red triangles), 0.7 wt % (green squares), and 2.8 wt % (blue inverted triangles) PVP as ETL. Inset: $J-V$ response in dark. (b) FF (red circles) and η (blue triangles) of devices as a function of PVP concentration. (c) $J-V$ response at AM1.5G 100 mW/cm^2 for conventional devices using nothing (black circles), ZnO NP with 0.14 wt % PVP (red triangles), and ZnO NP with 0.7 wt % PVP (green squares) as ETL.

value but is the result of lower performance due to higher R_s found in the higher PVP concentration films arising from a PVP overlayer. Similarly, Small et al. attributed the reduction in FF in their OPV devices without UV-ozone treatment to the presence of a continuous PVP on the ZnO sol-gel film.[14] The optimal PVP concentration of 0.7 wt % yields high R_p and low R_s, leading to FF of 0.60 and η of 3.25%.

In addition, we show that the performance of conventional P3HT:PCBM OPV devices can be improved with the insertion of a ZnO NP:PVP ETL layer between the active layer and the top Al cathode (Figure 4c). Compared to the control device with no ETL (Figure 4c, black circles), the device with ZnO NP:PVP (0.14 wt %) (Figure 4c, red triangles) exhibited an increase in V_{oc} and FF, leading to an improvement in η from 1.42 to 2.34% (Table 1). However, an increase in PVP concentration to 0.7 wt % (Figure 4c, green squares) caused FF to again decrease. This trend is reflected in the R_s for the devices, decreasing from 25 Ω cm^2 for the control sample to 11 Ω cm^2 for the ZnO NP:PVP (0.14 wt %) device and then increasing to 13 Ω cm^2 for the ZnO NP:PVP (0.7 wt %) device (Table 1). The correlation between optimal polymer concentration and maximum device FF is qualitatively similar to a previous report using ZnO NP:PEO ETLs.[13] In short, we demonstrate effective ETLs formed from spin coating of ZnO NP:PVP suspensions without further processing for both conventional and inverted P3HT:PCBM devices.

We further examine the effect of ZnO NP:PVP and ZnO NP:DEA Φ on inverted P3HT:ICBA OPV devices and compare with P3HT:PCBM devices. P3HT:ICBA devices with ZnO NP:PVP (Figure 5a) and ZnO NP:DEA (Figure 5b) ETLs exhibited J_{sc} and FF largely independent of PVP or DEA concentration. However, V_{oc} increased from 0.75 to 0.82 V as PVP concentration increased from 0 to 0.7 wt % and from 0.70 to 0.77 V as DEA concentration increased from 0 to 0.01 M (Table 2), resulting from an increased built-in field in the bulk heterojunction active layer due to decreased ETL work function. We should note that the similar dark and light $J-V$ curves for P3HT:ICBA devices using ZnO NP:PVP ETL (Figure 5a) and ZnO NP:DEA ETL (Figure 5b) suggest that the shape of the ZnO NP does not significantly affect OPV performance. Figure 5c shows that V_{oc} of P3HT:ICBA devices increases linearly as ETL Φ decreases through the addition of either PVP (solid red circles) or DEA (open red circles), with a slope of −0.2. In comparison, V_{oc} of P3HT:PCBM devices increases as ZnO NP:PVP ETL Φ decreases with a similar slope of −0.25, and saturates at 0.56 V when Φ falls below 4.1 eV (Figure 5c, solid blue triangles); these slopes match well with published results for P3HT:PCBM devices using ETLs of sol-gel ZnO films modified with self-assembled monolayers with different terminal groups,[16] indicating that such behavior may be characteristic of contact layers with interfacial dipoles. However, our synthetic method is much simpler, and offers the ability to tune Φ by changing the nature and concentration of the organic additive. The weak dependence of V_{oc} on ETL Φ is similar to results reported by Brabec et al.,[17] and can be attributed to Fermi level pinning between the acceptor and ETL.[18,19] As the ETL Φ becomes sufficiently low, other factors

Table 1. Performance Parameter Comparison of Inverted and Conventional P3HT:PCBM Devices with ZnO:PVP ETLs under AM 1.5G 100 mW/cm^2, as Shown in Figure 4a and c

arch.	PVP conc. (wt %)	V_{oc} (V)	J_{sc} (mA/cm^2)	FF	η (%)	R_s (Ω cm^2)	R_p (kΩ cm^2)
inv.	0	0.51 ± 0.01	9.53 ± 0.18	0.47 ± 0.01	2.27 ± 0.03	6 ± 2	31 ± 13
	0.14	0.55 ± 0.01	9.76 ± 0.18	0.59 ± 0.03	3.12 ± 0.14	6 ± 3	60 ± 24
	0.7	0.56 ± 0.00	9.74 ± 0.30	0.60 ± 0.03	3.25 ± 0.04	6 ± 2	653 ± 381
	2.8	0.56 ± 0.00	8.38 ± 0.67	0.31 ± 0.05	1.45 ± 0.32	20 ± 8	420 ± 76
conv.	no ETL	0.38 ± 0.00	8.29 ± 0.14	0.45 ± 0.00	1.42 ± 0.03	25 ± 2	129 ± 64
	0.14	0.55 ± 0.01	8.43 ± 0.17	0.51 ± 0.02	2.34 ± 0.15	11 ± 2	406 ± 340
	0.7	0.56 ± 0.00	8.24 ± 0.19	0.44 ± 0.01	2.03 ± 0.08	13 ± 2	319 ± 295

dx.doi.org/10.1021/am402511t | ACS Appl. Mater. Interfaces 2013, 5, 9128−9133

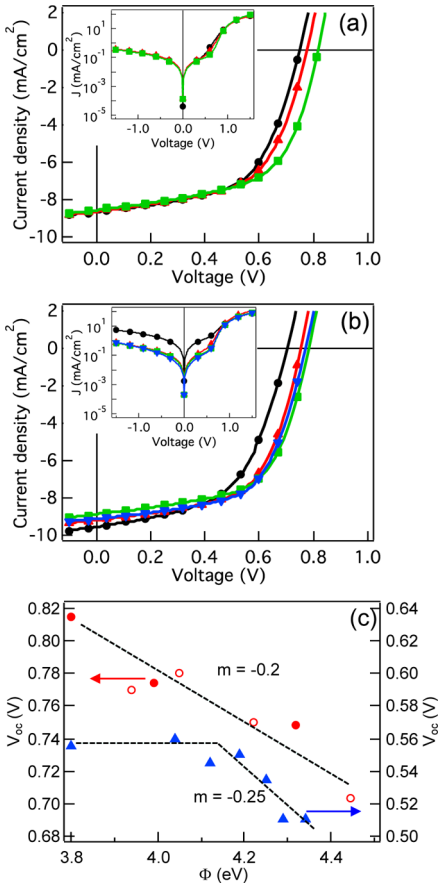

Figure 5. Performance of inverted P3HT:ICBA devices using ZnO NP:PVP and ZnO NP:DEA as ETL. (a) *J*−*V* response at AM1.5G 100 mW/cm^2 for devices using ZnO NP with 0 wt % (black circles), 0.14 wt % (red triangles), and 0.7 wt % (green squares) PVP as ETL. Inset: *J*−*V* response in dark. (b) *J*−*V* response at AM1.5G 100 mW/cm^2 for devices using ZnO NP with 0 M (black circles), 0.001 M (red triangles), 0.005 M (green squares), and 0.01 M (blue inverted triangles) DEA as ETL. Inset: *J*−*V* response in dark. (c) V_{oc} of P3HT:ICBA with ZnO NP:PVP (solid red circles), P3HT:ICBA with ZnO NP:DEA (open red circles), and P3HT:PCBM with ZnO NP:PVP (solid blue triangles) devices as a function of ETL Φ.

begin to affect the device performance. The saturation of V_{oc} for P3HT:PCBM devices indicates the V_{oc} ultimately is limited by energy offset between the donor and acceptor, not by the contacts, due to a higher electron affinity of PCBM (3.8 eV)[20] compared to ICBA (3.57 eV).[21] Our results also suggest that further improvements in V_{oc} for P3HT:ICBA devices may be possible by optimizing ETL Φ.

CONCLUSIONS

In conclusion, we demonstrate a simple and effective method to fabricate ETLs with tunable work function by spin coating ZnO NP:PVP and ZnO NP:DEA suspensions to form nanocomposite films. The improved performance arises from our ability to tune the electron transport layer's work function, hence increasing the built-in field in the device. Modification of ZnO NP surface with PVP or DEA induced a decrease in Φ from 4.4 to 3.95 eV, suggesting that the decrease was caused by an interfacial dipole. DEA addition yielded spherical nanoparticles, reduced size, and more uniform work function compared to PVP. Optimization of PVP concentration significantly improved FF and device efficiency of inverted P3HT:PCBM OPV devices. Conventional P3HT:PCBM OPV devices with good performance were realized by deposition of ZnO NP:PVP directly on top of the active layer, without the need for additional purification or thermal processing. Finally, the decrease in work function with increasing PVP or DEA concentration resulted in an increase in V_{oc} of inverted P3HT:ICBA and P3HT:PCBM devices, with a small slope consistent with Fermi level pinning between acceptor and ETL. The concept of solution processed films of nanoparticle:organic hybrid nanocomposites can be easily extended to other combinations to create interfacial contact layers with tunable electronic properties for optimal OPV device performance.

AUTHOR INFORMATION

Corresponding Author

*E-mail: yjalee@utdallas.edu.

Notes

The authors declare no competing financial interest.

ACKNOWLEDGMENTS

This project is supported by the University of Texas at Dallas. J.W.P.H. acknowledges the Texas Instruments Distinguished Chair in Nanoelectronics. S.R.C. acknowledges the George A. Jeffrey NanoExplorers program at the University of Texas at Dallas.

REFERENCES

(1) Steim, R.; Kogler, F. R.; Brabec, C. J. *J Mater. Chem.* **2010**, *20*, 2499−2512.
(2) Yip, H.-L.; Jen, A. K. Y. *Energy Environ. Sci.* **2012**, *5*, 5994−6011.
(3) Waldauf, C.; Morana, M.; Denk, P.; Schilinsky, P. *Appl. Phys. Lett.* **2006**, *89*, 233517.
(4) Lee, K.; Kim, J. Y.; Park, S. H.; Kim, S. H.; Cho, S.; Heeger, A. J. *Adv. Mater.* **2007**, *19*, 2445−2449.
(5) Kim, J. Y.; Lee, K.; Coates, N. E.; Moses, D.; Nguyen, T.-Q.; Dante, M.; Heeger, A. J. *Science* **2007**, *317*, 222−225.

Table 2. Performance Parameter Comparison of Inverted P3HT:ICBA Devices with ZnO:PVP and ZnO:DEA ETLs at AM 1.5G 100 mW/cm^2, as Shown in Figure 5a and b

PVP conc. (wt %)	V_{oc} (V)	J_{sc} (mA/cm^2)	FF	η (%)	R_s (Ω cm^2)	R_p (kΩ cm^2)
0	0.75 ± 0.00	8.65 ± 0.23	0.58 ± 0.01	3.75 ± 0.08	6 ± 2	5.5 ± 1.8
0.14	0.77 ± 0.01	8.64 ± 0.10	0.58 ± 0.01	3.89 ± 0.08	7 ± 2	5.2 ± 1.5
0.7	0.82 ± 0.01	8.56 ± 0.40	0.59 ± 0.01	4.11 ± 0.20	6 ± 2	6.1 ± 1.3
DEA conc. (M)	V_{oc} (V)	J_{sc} (mA/cm^2)	FF	η (%)	R_s (Ω cm^2)	R_p (kΩ cm^2)
0	0.70 ± 0.00	9.55 ± 0.29	0.54 ± 0.01	3.65 ± 0.11	9 ± 1	1.5 ± 1.6
0.001	0.75 ± 0.00	9.18 ± 0.32	0.59 ± 0.01	4.09 ± 0.09	6 ± 2	3.5 ± 1.0
0.005	0.78 ± 0.00	8.87 ± 0.22	0.61 ± 0.01	4.19 ± 0.14	7 ± 2	3.8 ± 0.5
0.01	0.77 ± 0.00	9.11 ± 0.25	0.60 ± 0.01	4.22 ± 0.15	9 ± 1	7.0 ± 2.3

(6) Gilot, J.; Wienk, M. M.; Janssen, R. A. J. *Appl. Phys. Lett.* **2007**, *90*, 143512.
(7) Hau, S. K.; Yip, H.-L.; Baek, N. S.; Zou, J.; O'Malley, K.; Jen, A. K. Y. *Appl. Phys. Lett.* **2008**, *92*, 253301.
(8) Ferreira, S. R.; Lu, P.; Lee, Y.-J.; Davis, R. J.; Hsu, J. W. P. *J Phys. Chem. C* **2011**, *115*, 13471−13475.
(9) Zhang, F.; Ceder, M.; Inganas, O. *Adv. Mater.* **2007**, *19*, 1835−1838.
(10) Kang, H.; Hong, S.; Lee, J.; Lee, K. *Adv. Mater.* **2012**, *24*, 3005−3009.
(11) Zhou, Y.; Fuentes-Hernandez, C.; Shim, J.; Meyer, J.; Giordano, A. J.; Li, H.; Winget, P.; Papadopoulos, T.; Cheun, H.; Kim, J.; Fenoll, M.; Dindar, A.; Haske, W.; Najafabadi, E.; Khan, T. M.; Sojoudi, H.; Barlow, S.; Graham, S.; Bredas, J.-L.; Marder, S. R.; Kahn, A.; Kippelen, B. *Science* **2012**, *336*, 327−332.
(12) Steim, R.; Choulis, S. A.; Schilinsky, P.; Brabec, C. J. *Appl. Phys. Lett.* **2008**, *92*, 093303.
(13) Jo, S. B.; Lee, J. H.; Sim, M.; Kim, M.; Park, J. H.; Choi, Y. S.; Kim, Y.; Ihn, S.-G.; Cho, K. *Adv. Energy Mater.* **2011**, *1*, 690−698.
(14) Small, C. E.; Chen, S.; Subbiah, J.; Amb, C. M.; Tsang, S.-W.; Lai, T.-H.; Reynolds, J. R.; So, F. *Nat. Photonics* **2012**, *6*, 115−120.
(15) Bilecka, I.; Djerdj, I.; Niederberger, M. *Chem. Commun.* **2008**, 886−888.
(16) Ha, Y. E.; Jo, M. Y.; Park, J.; Kang, Y.-C.; Yoo, S. I.; Kim, J.-H. *J Phys. Chem. C* **2013**, *117*, 2646−2652.
(17) Brabec, C. J.; Cravino, A.; Meissner, D.; Sariciftci, N. S.; Fromherz, T.; Rispens, M. T.; Sanchez, L.; Hummelen, J. C. *Adv. Funct. Mater.* **2001**, *11*, 374−380.
(18) Braun, S.; Salaneck, W. R.; Fahlman, M. *Adv. Mater.* **2009**, *21*, 1450−1472.
(19) Davis, R. J.; Lloyd, M. T.; Ferreira, S. R.; Bruzek, M. J.; Watkins, S. E.; Lindell, L.; Sehati, P.; Fahlman, M.; Anthony, J. E.; Hsu, J. W. P. *J. Mater. Chem.* **2011**, *21*, 1721−1729.
(20) Guan, Z.-L.; Kim, J. B.; Wang, H.; Jaye, C.; Fischer, D. A.; Loo, Y.-L.; Kahn, A. *Org. Electron.* **2010**, *11*, 1779−1785.
(21) Guan, Z.-L.; Bok Kim, J.; Loo, Y.-L.; Kahn, A. *J. Appl. Phys.* **2011**, *110*, 043719.